Energy-Efficient THz NOMA for SWIPT-aided Miniature UAV Networks

Jalal Jalali *Member, IEEE*, Ata Khalili *Member, IEEE*, Hina Tabassum *Senior Member, IEEE*, Rafael Berkvens *Member, IEEE*, Jeroen Famaey *Senior Member, IEEE*, and Walid Saad *Fellow, IEEE*.

***Abstract*—This paper focuses on maximizing the energy efficiency (EE) of a cooperative network involving miniature unmanned aerial vehicles (UAV) operating at terahertz (THz) frequencies, leveraging simultaneous wireless information and power transfer (SWIPT). In this context, the considered system encompasses a source node that adopts SWIPT, thereby allowing the miniature UAV to receive information and power simultaneously. The harvested energy is then employed to relay data to designated destination nodes. The EE of the system is maximized by optimizing non-orthogonal multiple access (NOMA) power allocation coefficients, SWIPT power splitting (PS) ratios, and UAV's trajectory. This optimization problem is solved in two stages. First, the PS ratios and trajectory are optimized using a successive convex approximation. Next, NOMA power coefficients are optimized using a quadratic transform approach. Simulation results validate the effectiveness of the proposed algorithm compared to baselines.**

***Index Terms*—EE, NOMA, SWIPT, THz, UAV.**

I. Introduction

MINIATURIZED unmanned aerial vehicles (UAVs) have recently attracted substantial attention due to distinctive capabilities in exploring uncharted and complex environments and maneuvering through confined areas [1]. Given the small size of miniature UAVs, they often come with limited energy resources and have a significant energy consumption, necessitating energy-efficient designs. Within this context, simultaneous wireless information and power transfer (SWIPT) [2] is viewed as a transformative technique capable of not only improving the information transfer rate but also extending the miniature UAV's endurance time, thus improving the overall UAV network's energy efficiency (EE).

To date, several prior works have considered throughput, coverage, or reliability maximization in SWIPT-assisted UAV networks. In [3], UAV-assisted cooperative communication was studied where throughput was maximized under the UAV's mobility and harvested power constraints. Also, in [4], the performance of downlink UAV-assisted SWIPT was analyzed in terms of security, reliability, and coverage. However, since future wireless networks are expected to accommodate massive connectivity and extreme data rates [5], the integration of sophisticated wireless technologies into UAV networks becomes essential. Therefore, harnessing the combined advantages of the vast bandwidth available at the terahertz (THz) spectrum along with the capabilities of non-orthogonal multiple access (NOMA) is imperative [6].

Recent studies have explored the concept of THz-enabled UAV communications [7]–[10]. In [7] and [8], authors considered UAV-assisted THz networks, with [7] detailing how UAVs serve as static relays for maximizing transmission capacity, and [8] discussing the optimization of UAV placement, power control, and bandwidth allocation to enhance data rates. Conversely, the authors in [9] developed a cooperative recharging-transmission strategy for UAV-aided THz downlink networks, where UAVs harvest energy from a wireless charging base station. In [10], a deep reinforcement learning algorithm was employed to minimize energy consumption and delay with the joint optimization of trajectory and resource allocation for sub-THz multi-access edge computing-enabled UAV.

None of the prior works [7]–[10] addressed EE optimization in THz-NOMA-enabled UAV networks with or without SWIPT. The main contribution of this paper is to fill this gap by proposing a novel framework for maximizing EE in a SWIPT-aided miniature UAV network operating at THz frequencies. In particular, this paper introduces a model in which a source node sends a superimposed message to the UAV and a destination node, using different power coefficients in NOMA. The signal received at the UAV is then split into two components using power splitting (PS). One portion of the signal is for energy harvesting (EH), and the other for information decoding (ID). An optimization problem is formulated for controlling the NOMA power allocation coefficients, SWIPT PS ratios, and UAV trajectory. This problem is a fractional programming problem with a non-linear sum of ratios, and thus, needs to be decomposed into two stages. First, the PS ratios and trajectories are optimized using successive convex approximation. In the second stage, NOMA power coefficients are optimized using a quadratic transform approach. Numerical results show up to 30.3% improvement in EE compared to baseline methods, highlighting its superiority over OMA and evaluating the impact of molecular absorption on EE. This makes the UAV trajectory optimization unique and enhances overall network performance.

II. System Model and Problem Formulation

We consider a downlink transmission miniature UAV-aided SWIPT NOMA cooperative system. As shown in Fig. 1, a source node transmits information to two nodes: A miniature UAV and a destination. The UAV acts as an EH aerial relay to ensure the high targeted rate of the destination node. A three-dimensional (3D) Cartesian coordinate system is considered in which the source and destination nodes are placed at $\boldsymbol{s}(t) = [s_x(t), s_y(t), H_1]^{\mathrm{T}} \in \mathbb{R}^{3\times 1}$ and $\boldsymbol{d}(t) = [d_x(t), d_y(t), 0]^{\mathrm{T}} \in \mathbb{R}^{3\times 1}$, respectively, where $[\cdot]^{\mathrm{T}}$ is the transpose operation. The destination node is static on the ground, while the UAV and source are at fixed, yet different, heights above the ground. The instantaneous coordinates of the UAV are given by $\boldsymbol{q}(t) = [x(t), y(t), H_2]^{\mathrm{T}} \in \mathbb{R}^{3\times 1}$ at time $0 < t < T$. The UAV's total flying time T is divided into N time slots of fixed duration, where $\boldsymbol{q}[n], \forall n \in \{1, ..., N\}$ is the sampled trajectory. Each time slot is assumed to be sufficiently small such that the UAV location can be considered approximately constant, facilitating

Jalal Jalali, Rafael Berkvens, and Jeroen Famaey are with IDLab research group, University of Antwerp - imec, 2000 Antwerp, Belgium (e-mail: {jalal.jalali, rafael.berkvens, jeroen.famaey}@imec.be). Ata Khalili is with Friedrich-Alexander-University, Erlangen, Germany (e-mail: ata.khalili@ieee.org). Hina Tabassum is with York University, Toronto, Canada (e-mail: Hina.Tabassum@lassonde.yorku.ca). Walid Saad is with Wireless@VT, Virginia Tech, USA (e-mail: walids@vt.edu). Walid Saad is also with Artificial Intelligence & Cyber Systems Research Center, Lebanese American University.

This work was supported by the CHIST-ERA grant (CHIST-ERA-20-SICT-003), with FWO (V478223N), ANR, NKFIH, and UKRI funding, and in part, by the U.S. National Science Foundation under Grant CNS-2225511.

the trajectory and resource allocation design. The constraints related to the UAV position and maximum speed are:

$$\boldsymbol{q}[1] = \boldsymbol{q}_s, \tag{1a}$$
$$\boldsymbol{q}[N+1] = \boldsymbol{q}_e, \tag{1b}$$
$$\|\boldsymbol{q}[n+1] - \boldsymbol{q}[n]\| \leq \varpi V_{\max}, \ \forall n, \tag{1c}$$

where $V_{\max}$ is the maximum flying velocity, ϖ is the duration of each time slot, and $\boldsymbol{q}_s$ and $\boldsymbol{q}_e$ are the first and final UAV positions, respectively. The channel gain between source-to-UAV and UAV-to-destination, denoted by $h_{sr}[n]$ and $h_{rd}[n]$, follow the free-space path loss model and are given by:

$$h_{sr}[n] = \frac{\beta_0}{\|\boldsymbol{q}[n] - \boldsymbol{s}[n]\|} e^{-\frac{\xi(f)}{2}\|\boldsymbol{q}[n]-\boldsymbol{s}[n]\|}, \forall n, \tag{2}$$
$$h_{rd}[n] = \frac{\beta_0}{\|\boldsymbol{q}[n] - \boldsymbol{d}[n]\|} e^{-\frac{\xi(f)}{2}\|\boldsymbol{q}[n]-\boldsymbol{d}[n]\|}, \forall n, \tag{3}$$

where $\xi(f)$ is a molecular absorption coefficient that is influenced by the operating frequency f and the concentration of water vapor molecules. To simplify the notation, we will henceforth denote $\xi(f)$ as ξ. And, $\beta_0 = c/4\pi f$ is the reference power gain, where c is the speed of light [9]. The channel power gain $h_{sd}[n]$ between the source-to-destination follows the same structure, as in (2) and (3) [11].

Cooperative communication is executed in two phases. In the first phase, the UAV harvests energy and decodes information from the source node while the destination node receives its respective data. In the second phase, the UAV acts as an aerial relay to re-transmit the destination node's data using the harvested power of the first phase.

A. Phase One: Direct Transmission

In this phase, the source transmits the information to both the miniature UAV and destination node by exploiting power-domain NOMA. Hence, the transmit signal is given by:

$$s[n] = \sqrt{\alpha_1[n]}s_1[n] + \sqrt{\alpha_2[n]}s_2[n], \forall n, \tag{4}$$

where $s_1[n]$ and $s_2[n]$ are transmit symbols during each time slot and assumed to be independently circularly symmetric complex Gaussian (CSCG) distributed with zero mean and unit variance. Moreover, $\sqrt{\alpha_1[n]}$ and $\sqrt{\alpha_2[n]}$ represent the NOMA power allocation coefficients in the n-th time slot, which need to satisfy the two following constraints:

$$\alpha_1[n] + \alpha_2[n] \leq P_{\text{peak}}, \forall n, \tag{5a}$$
$$\frac{1}{N}\sum_{n=1}^{N} \alpha_1[n] + \alpha_2[n] \leq P_{\max}, \tag{5b}$$

where P_{peak} represents the peak power that the source can deliver in any individual time slot and $P_{\max}$ is the maximum power constraint that must be maintained across all time slots. The received signal at the UAV will be:

$$y_r^{(1)}[n] = h_{sr}[n]s[n] + z_1^{(1)}[n], \forall n, \tag{6}$$

where $z_1^{(1)}[n] \sim \mathcal{N}(0, \sigma_1^2)$ is the received CSCG noise at the UAV node. By adopting a PS-SWIPT architecture, the received signal for ID and EH from the radio frequency (RF) source can be expressed as:

$$y_{\text{EH}}^{(1)}[n] = \sqrt{\rho[n]}\big(y_r^{(1)}[n]\big), \forall n, \tag{7}$$
$$y_{\text{ID}}^{(1)}[n] = \sqrt{1-\rho[n]}\big(y_r^{(1)}[n]\big) + z_2^{(1)}[n], \forall n, \tag{8}$$

where $0 < \rho[n] < 1$ is the PS ratio, and $z_2^{(1)}[n] \sim \mathcal{N}(0, \sigma_2^2)$ is the additional noise caused by the ID receiver. The UAV node

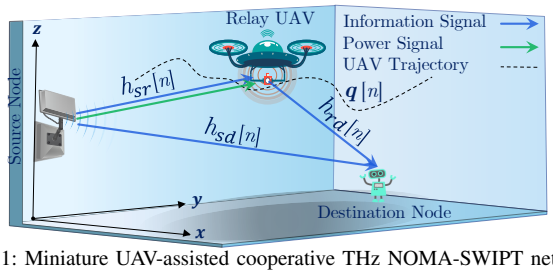

Fig. 1: Miniature UAV-assisted cooperative THz NOMA-SWIPT network.

employs a successive interference cancellation (SIC) receiver to decode the signals. In fact, the miniature UAV first decodes the data of the destination node and then removes it from its received signal to obtain its own data in a successive manner. The received signal-to-interference-plus-noise-ratio (SINR) at the UAV to detect $s_2[n]$ can be stated as:

$$\gamma_{d\leftarrow r}^{(1)}[n] = \frac{(1-\rho[n])\alpha_2[n]|h_{sr}[n]|^2}{(1-\rho[n])\alpha_1[n]|h_{sr}[n]|^2 + \Pi[n]}, \forall n, \tag{9}$$

where $\Pi[n] = (1-\rho[n])\sigma_1^2[n] + \sigma_2^2[n]$ is the total equivalent noise. Then, the corresponding SINR to decode UAV's data can be described as:

$$\gamma_r^{(1)}[n] = \frac{(1-\rho[n])\alpha_1[n]|h_{sr}[n]|^2}{\Pi[n]}, \forall n. \tag{10}$$

According to (6) and (7), the RF harvested power at the UAV by ignoring the noise power can be expressed as:

$$E[n] = \eta\rho[n]|h_{sr}[n]|^2\tau[n], \forall n, \tag{11}$$

where $\eta \in (0, 1]$ is the energy conversion efficiency and $\tau[n]$ is the transmission time fraction for the first phase during the n-th time slot, assuming the transmission duration is the same for two phases, i.e., $\tau[n] = \frac{1}{2}$. Consequently, the UAV's transmit power, enabled by the harvested energy, is described as [3]:

$$P_t[n] = \frac{E[n]}{1-\tau[n]}, \forall n. \tag{12}$$

The received signal at the destination can be stated as:

$$y_d^{(1)}[n] = h_{sd}[n]s[n] + {\nu_1}^{(1)}[n], \forall n, \tag{13}$$

where ${\nu_1}^{(1)}[n] \sim \mathcal{N}(0, \delta_1^2[n])$ is the received noise at the destination node in the first phase. The SINR at the destination node to decode its own data can be written as:

$$\gamma_d^{(1)}[n] = \frac{\alpha_2[n]\ |h_{sd}[n]|^2}{\alpha_1[n]\ |h_{sd}[n]|^2 + \delta_1^2[n]}, \forall n. \tag{14}$$

B. Phase Two: Cooperative Transmission

In this phase, the UAV uses the harvested power to transmit the data of the destination node[1]. Hence, the received signal at the destination node will be:

$$y_d^{(2)}[n] = \sqrt{P_t[n]}h_{rd}[n]s_2[n] + {\nu_2}^{(2)}[n], \forall n, \tag{15}$$

where ${\nu_2}^{(2)}[n] \sim \mathcal{N}(0, \delta_2^2[n])$ is the received noise at the destination node. The corresponding SINR reads as:

$$\gamma_d^{(2)}[n] = \frac{\eta\rho[n]|h_{sr}[n]|^2|h_{rd}[n]|^2}{\delta_2^2[n]}, \forall n. \tag{16}$$

Ultimately, the destination node uses maximal ratio combination (MRC) to integrate the transmit signals from the two phases. The corresponding SINR can be represented as:

$$\gamma_d^{\text{MRC}}[n] = \gamma_d^{(1)}[n] + \gamma_d^{(2)}[n], \forall n. \tag{17}$$

C. Problem Formulation

We first define the network's EE as the ratio of the sum rate to the total network's power consumption. That is $\eta_{EE}[n] =$

[1] In Phase Two, we assume no transmission from the source to save the overall network's energy consumption, enhancing the miniature UAV relay efficiency.

$\frac{R_{\text{sum}}[n]}{P_{\text{sum}}[n]}$, where $R_{\text{sum}}[n] = \log_2(1+\gamma_r^1[n]) + \log_2(1+\gamma_d^{\text{MRC}}[n])$. Considering a constant miniature UAV's flying power P_c, the total transmission power of the system will be $P_{\text{sum}}[n] = \alpha_1[n] + \alpha_2[n] - P_t[n] + P_c$. To maximize EE by optimizing the NOMA power allocation coefficients, PS ratio, and UAV trajectory, the following problem is formulated:

$$\mathrm{P}_1: \max_{\rho[n],\alpha_1[n],\alpha_2[n],\boldsymbol{q}[n]} \sum_{n=1}^{N} \eta_{EE}[n] \tag{18}$$

$$s.t.: \ \frac{1}{N}\sum_{n=1}^{N} P_t[n] \geq \frac{1}{N}\sum_{n=1}^{N} P[n], \tag{18a}$$

$$\gamma_{d\leftarrow r}^{(1)}[n] \geq \gamma_{\min}[n], \ \forall n, \tag{18b}$$

$$\gamma_d^{\text{MRC}}[n] \geq \Gamma_{\min}[n], \ \forall n, \tag{18c}$$

$$0 < \rho[n] < 1, \ \forall n, \tag{18d}$$

$$P[n] \geq 0, \ \forall n, (1a)-(1c), (5a), (5b). \tag{18e}$$

Constraint (18a) ensures that the power harvested at the UAV for all time slots is bigger than a minimum harvested power $P[n] = \frac{E[n]}{\tau[n]}$ (we consider $P[n] = P_{\text{EH}}$, i.e., the harvested power). (18b) confirms the successful decoding of the destination node's data at the UAV is bigger than a threshold $\gamma_{\min}[n]$, while (18c) ensures the minimum required SINR for the destination node to be at least $\Gamma_{\min}[n]$, where $\Gamma_{\min} \geq \gamma_{\min}$. The PS-SWIPT ratio and the feasibility of the UAV's transmitted power are constrained by (18d) and (18e)[2].

III. A Two-Stage Solution to EE Problem

P_1 is non-convex NP-hard due to coupling of optimization variables. The objective function of P_1 is in the form of sum-of-ratios, which is incompatible with conventional Dinkelbach method solutions [12]. We propose a two-stage solution, allowing for independent optimization of each variable.

A. Stage-one: Optimizing PS ratio and UAV trajectory

In this stage, the PS ratio and UAV's trajectory are designed with fixed NOMA power allocation coefficients. The sum rate function is non-convex due to the coupling between optimization variables. Nonetheless, the non-linear fractional objective function first needs to be transformed into a subtractive form by utilizing the following theorem from [13].

Theorem [13]: Suppose that $\rho^*[n]$ and $\boldsymbol{q}^*[n]$ are the optimal solutions to the problem P_1. Then, the following optimization problem can provide an optimal solution in the existence of two vectors, namely, $\boldsymbol{\lambda} = [\lambda_1^*, ..., \lambda_N^*]^T$ and $\boldsymbol{\psi} = [\psi_1^*, ..., \psi_N^*]^T$ as follows:

$$\max_{\rho[n],\boldsymbol{q}[n]} \sum_{n=1}^{N} \lambda_n^* \big[R_{\text{sum}}[n] - \psi_n^*(P_{\text{sum}}[n])\big]. \tag{19}$$

Furthermore, $\rho^*[n]$ and $\boldsymbol{q}^*[n]$ meet the following equations:

$$R_{\text{sum}}^*[n] - \psi_n^*(P_{\text{sum}}[n]) = 0, \forall n, \tag{20}$$

$$1 - \lambda_n^*(P_{\text{sum}}[n]) = 0, \forall n. \tag{21}$$

Specifically, the equivalent subtractive form in (19) with the additional parameters $\{\boldsymbol{\lambda}^*, \boldsymbol{\psi}^*\}$ has the same optimal solution as P_1 for given $\alpha_1[n]$ and $\alpha_2[n]$. In particular, the problem (19) can be solved iteratively with a two-layer approach, i.e., inner and outer layers. In the inner layer, (19) is solved under given $\boldsymbol{\lambda}$ and $\boldsymbol{\psi}$. Then, the two equations (20) and (21) are updated in the outer layer to obtain $\{\boldsymbol{\lambda}^*, \boldsymbol{\psi}^*\}$.

[2]Distance impacts the molecular absorption coefficient, setting P_1 apart from UAV location optimization problems that do not account for THz channels.

*1) **Inner-layer Problem**:* The inner layer optimization problem is non-convex. Therefore, we first optimize the PS ratio while considering a predetermined UAV trajectory and fixed NOMA power coefficients. Thus, the optimization problem for the PS ratio can be formulated as follows:

$$\mathrm{P}_2: \max_{\rho[n]} \sum_{n=1}^{N} \lambda_n^* \big[R_{\text{sum}}[n] - \psi_n^*(P_{\text{sum}}[n])\big] \tag{22}$$

$$s.t.: \quad (18b) - (18d).$$

The problem P_2 is convex with respect to $\rho[n]$ and can be solved efficiently. Subsequently, we optimize the trajectory under the optimal PS ratio as follows:

$$\mathrm{P}_3: \max_{\boldsymbol{q}[n]} \sum_{n=1}^{N} \lambda_n^* \big[R_{\text{sum}}[n] - \psi_n^*(P_{\text{sum}}[n])\big] \tag{23}$$

$$s.t.: \quad \sum_{n=1}^{N} \frac{\eta\rho[n]\beta_0^2 e^{-\xi(\|\boldsymbol{q}[n]-\boldsymbol{s}[n]\|)}}{\|\boldsymbol{q}[n]-\boldsymbol{s}[n]\|^2} \geq \sum_{n=1}^{N} P[n], \tag{23a}$$

$$\frac{\alpha_2[n]}{\alpha_1[n]+x\|\boldsymbol{q}[n]-\mathbf{s}[n]\|^2 \tilde{e}^{\xi(\|\boldsymbol{q}[n]-\boldsymbol{s}[n]\|)}} \geq \gamma_{\min}[n], \ \forall n, \tag{23b}$$

$$\frac{\eta\rho[n]\beta_0^4}{\delta_2^2[n]} \cdot \frac{e^{-\xi(\|\boldsymbol{q}[n]-\boldsymbol{s}[n]\|+\|\boldsymbol{q}[n]-\boldsymbol{d}[n]\|)}}{\|\boldsymbol{q}[n]-\boldsymbol{s}[n]\|^2 \|\boldsymbol{q}[n]-\boldsymbol{d}[n]\|^2} + \frac{\alpha_2[n]\ |h_{sd}[n]|^2}{\alpha_1[n]\ |h_{sd}[n]|^2+\delta_1^2[n]} \geq \Gamma_{\min}[n], \ \forall n, (1a)-(1c), (18e), \tag{23c}$$

where $x = \frac{\Pi[n]}{1-\rho[n]\beta_0^2}$. The problem P_3 is still non-convex. Hence, P_3 is transformed into its equivalent form by introducing slack optimization variables as follows:

$$\mathrm{P}_4: \max_{\boldsymbol{q}[n],v[n],t[n],a[n],b[n]} \sum_{n=1}^{N} \lambda_n^* \big[R_{\text{sum}}[n] - \psi_n^*(P_{\text{sum}}[n])\big] \tag{24}$$

$$s.t.: \quad \sum_{n=1}^{N} \frac{\eta\rho[n]\beta_0^2}{e^{a[n]}} \geq \sum_{n=1}^{N} P[n], \tag{24a}$$

$$\frac{\alpha_2[n]}{\alpha_1[n]+xe^{a[n]}} \geq \gamma_{\min}[n], \ \forall n, \tag{24b}$$

$$\frac{\alpha_2[n]\ |h_{sd}[n]|^2}{\alpha_1[n]\ |h_{sd}[n]|^2+\delta_1^2[n]} + \frac{\eta\rho[n]\beta_0^4}{\delta_2^2[n]e^{a[n]+b[n]}} \geq \gamma_{\min}[n], \forall n, \tag{24c}$$

$$v[n] \leq \frac{\|\boldsymbol{q}[n]-\boldsymbol{s}[n]\|^2}{e^{-\xi\|\boldsymbol{q}[n]-\boldsymbol{s}[n]|}}, \ t[n] \leq \frac{\|\boldsymbol{q}[n]-\boldsymbol{d}[n]\|^2}{e^{-\xi\|\boldsymbol{q}[n]-\boldsymbol{d}[n]\|}}, \forall n, \tag{24d}$$

$$v[n] \leq e^{a[n]}, \quad t[n] \leq e^{b[n]}, \forall n, (1a)-(1c), (18e), \tag{24e}$$

where

$$R_{\text{sum}}[n] = \log_2\left(1 + \left(\frac{(1-\rho[n])\alpha_1[n]\beta_0^2}{\Pi[n]} \cdot \frac{1}{e^{a[n]}}\right)\right) + \log_2\left(1 + \gamma_d^{(1)}[n] + \left(\frac{\eta\rho[n]\beta_0^4}{\delta_2^2[n]} \cdot \frac{1}{e^{a[n]+b[n]}}\right)\right). \tag{25}$$

Using the above transformations, the main objective function and constraints become convex, albeit intractable. Consequently, successive convex approximation (SCA)-based first-order Taylor expansions are exploited to approximate P_4 by convex ones. The first-order lower bounds are given by:

$$e^{a[n]} \geq e^{a^{(k)}[n]}(1 + a[n] - a^{(k)}[n]) \triangleq \tilde{e}^{a[n]}, \forall n, \tag{26}$$

$$e^{b[n]} \geq e^{b^{(k)}[n]}(1 + \ b[n] - b^{(k)}[n]) \triangleq \tilde{e}^{b[n]}, \forall n, \tag{27}$$

$$\frac{\|\boldsymbol{q}[n]-\boldsymbol{s}[n]\|^2}{e^{-\xi\|\boldsymbol{q}[n]-\boldsymbol{s}[n]\|}} \geq \frac{\left\|\boldsymbol{q}^{(k)}[n]-\boldsymbol{s}[n]\right\|^2}{e^{-\xi\left\|\boldsymbol{q}^{(k)}[n]-\boldsymbol{s}[n]\right\|}} + (2+\xi||\boldsymbol{q}^{(k)}[n]-\boldsymbol{s}[n]||)\cdot \frac{(\boldsymbol{q}^{(k)}[n]-\boldsymbol{s}[n])^T(\boldsymbol{q}[n]-\boldsymbol{q}^{(k)}[n])}{e^{-\xi\left\|\boldsymbol{q}^{(k)}[n]-\boldsymbol{s}[n]\right\|}} \triangleq \frac{\|\tilde{\boldsymbol{q}}[n]-\boldsymbol{s}[n]\|^2}{e^{-\xi\|\tilde{\boldsymbol{q}}[n]-\boldsymbol{s}[n]\|}}, \forall n, \tag{28}$$

$$L_{\varkappa}(\alpha_1[n],\alpha_2[n],\wp,\boldsymbol{\theta},\boldsymbol{\Theta},\boldsymbol{\mu},\boldsymbol{\vartheta})=\sum_{n=1}^{N}\iota[n]P_{\text{sum}}^2[n]+\frac{1}{2\varkappa}\Bigg[\Bigg(\Bigg[\sum_{n=1}^{N}\wp_n+\varkappa\Big(\frac{N}{1-\rho[n]}-\frac{\alpha_2[n]|h_{sr}[n]|^2}{\gamma_{\min}[n]}+\alpha_1[n]|h_{sr}[n]|^2\Big)\Bigg]^{+}\Bigg)^2+\sum_{n=1}^{N}\frac{1}{4\iota[n]\hat{R}_{\text{sum}}^2[n]}+\Bigg(\Bigg[\sum_{n=1}^{N}\theta_n+\varkappa(\delta_1^2[n]x-\alpha_2[n]|h_{sd}[n]|^2+\alpha_1[n]|h_{sd}[n]|^2x)\Bigg]^{+}\Bigg)^2+\Bigg(\Bigg[\sum_{n=1}^{N}\Theta_n+\varkappa(\alpha_1[n]+\alpha_2[n]-P_{\text{peak}})\Bigg]^{+}\Bigg)^2+\Bigg(\Bigg[\mu_n+\varkappa(\frac{1}{N}\sum_{n=1}^{N}\alpha_1[n]+\alpha_2[n]-P_{\max})\Bigg]^{+}\Bigg)^2+\Bigg(\Bigg[\sum_{n=1}^{N}\vartheta_n-\varkappa P[n]\Bigg]^{+}\Bigg)^2-\sum_{n=1}^{N}\wp_n^2-\sum_{n=1}^{N}\theta_n^2-\sum_{n=1}^{N}\Theta_n^2-\mu_n^2-\sum_{n=1}^{N}\vartheta_n\Bigg], \quad (41)$$

$$\frac{\|\boldsymbol{q}[n]-\boldsymbol{d}[n]\|^2}{e^{-\xi\|\boldsymbol{q}[n]-\boldsymbol{d}[n]\|^2}}\geq\frac{\|\boldsymbol{q}^{(k)}[n]-\boldsymbol{d}[n]\|^2}{e^{-\xi\|\boldsymbol{q}^{(k)}[n]-\boldsymbol{d}[n]\|}}+(2+\xi\|\boldsymbol{q}^{(k)}[n]-\boldsymbol{d}[n]\|)\cdot\frac{(\boldsymbol{q}^{(k)}[n]-\boldsymbol{d}[n])^T(\boldsymbol{q}[n]-\boldsymbol{q}^{(k)}[n])}{e^{-\xi\|\boldsymbol{q}^{(k)}[n]-\boldsymbol{d}[n]\|}}\triangleq\frac{\|\tilde{\boldsymbol{q}}[n]-\boldsymbol{d}[n]\|^2}{e^{-\xi\|\tilde{\boldsymbol{q}}[n]-\boldsymbol{d}[n]\|^2}},\forall n, \quad (29)$$

where $e^{a^{(k)}[n]}$ and $e^{b^{(k)}[n]}$ express the Taylor points at iteration k. Using above transformation,P_4 can be approximated as:

$$\text{P}_5:\max_{\boldsymbol{q}[n],v[n],t[n],a[n],b[n]}\sum\nolimits_{n=1}^{N}\lambda_n^*\big[\tilde{R}_{\text{sum}}[n]-\psi_n^*(P_{\text{sum}}[n])\big] \quad (30)$$

$$s.t.:\quad \sum\nolimits_{n=1}^{N}\frac{\eta\rho[n]\beta_0^2}{\tilde{e}^{a[n]}}\geq\sum\nolimits_{n=1}^{N}P[n], \quad (30a)$$

$$\frac{\alpha_2[n]}{\alpha_1[n]+x\tilde{e}^{a[n]}}\geq\gamma_{\min}[n],\ \forall n \quad (30b)$$

$$\frac{\alpha_2[n]\ |h_{sd}[n]|^2}{\alpha_1[n]|h_{sd}[n]|^2+\delta_1^2[n]}+\frac{\eta\rho[n]\beta_0^4}{\delta_2^2[n]\tilde{e}^{a[n]+b[n]}}\geq\gamma_{\min}[n],\forall n, \quad (30c)$$

$$v[n]\leq\frac{\|\tilde{\boldsymbol{q}}[n]-\boldsymbol{s}[n]\|^2}{e^{-\xi\|\tilde{\boldsymbol{q}}[n]-\boldsymbol{s}[n]\|}},t[n]\leq\frac{\|\tilde{\boldsymbol{q}}[n]-\boldsymbol{d}[n]\|^2}{e^{-\xi\|\tilde{\boldsymbol{q}}[n]-\boldsymbol{d}[n]\|}},\forall n, \quad (30d)$$

$$v[n]\leq\tilde{e}^{a[n]},\ t[n]\leq\tilde{e}^{b[n]},\forall n,(1a)-(1c),(18e), \quad (30e)$$

where $\tilde{R}_{\text{sum}}[n]=R_{\text{sum}}[n]|_{e^{a[n]}=\tilde{e}^{a[n]},e^{b[n]}=\tilde{e}^{b[n]}}$. P_5 can be solved by employing convex optimization solvers [12].

*2) **Outer-layer Problem**:* In this layer, the damped Newton method is utilized to find $\{\boldsymbol{\lambda},\boldsymbol{\psi}\}$. Let us define $\phi_n(\psi_n)=R_{\text{sum}}^*[n]-\psi_n^*(P_{\text{sum}}[n])$ and $\phi_{N+j}(\lambda_j)=1-\lambda_j^*(P_{\text{sum}}[j])$, $j\in\{1,...,N\}$. It is demonstrated in [2] that the optimal solution $\{\boldsymbol{\lambda}^*,\boldsymbol{\psi}^*\}$ is found if and only if $\phi(\boldsymbol{\lambda},\boldsymbol{\psi})=[\phi_1,\phi_2,...,\phi_{2N}]^T=0$. Accordingly, the updated value of the $\boldsymbol{\lambda}^{i+1}$ and $\boldsymbol{\psi}^{i+1}$ in the iteration i can be obtained by:

$$\boldsymbol{\lambda}^{i+1}=\boldsymbol{\lambda}^i+\zeta^i\boldsymbol{w}_{N+1:2N}^i,\qquad\boldsymbol{\psi}^{i+1}=\boldsymbol{\psi}^i+\zeta^i\boldsymbol{w}_{1:N}^i, \quad (31)$$

where $\boldsymbol{w}=[\dot{\phi}(\boldsymbol{\lambda},\boldsymbol{\psi})]^{-1}\phi(\boldsymbol{\lambda},\boldsymbol{\psi})$ with $\dot{\phi}(\boldsymbol{\lambda},\boldsymbol{\psi})$ as the Jacobian matrix of $\phi(\boldsymbol{\lambda},\boldsymbol{\psi})$, and ζ^i the largest value of Ξ^m satisfying $\|\phi(\boldsymbol{\lambda}^i+\Xi^m\boldsymbol{w}_{N+1:2N}^i,\boldsymbol{\psi}^i+\Xi^m\boldsymbol{w}_{1:N}^i)\|\leq(1-\varepsilon\Xi^m)\|\phi(\boldsymbol{\lambda},\boldsymbol{\psi})\|$, (32)

where $m\in\{1,2,...\}$, $\Xi^m\in(0,1)$, and $\varepsilon\in(0,1)$.

B. Stage-two: Optimizing power coefficients

A new framework is proposed in this stage. Consider a sum-fraction problem formulated as follows:

$$\min_{\boldsymbol{\Omega}\in C}\sum_{j=1}^{J}\frac{B_j(\boldsymbol{\Omega})}{A_j(\boldsymbol{\Omega})}, \quad (33)$$

where J is the maximum number of fractional terms, and $\boldsymbol{\Omega}$ is the optimization variable vector with the domain of C. One can prove (33) has an equivalent form as:

$$\min_{\boldsymbol{\Omega}\in C,\iota_j>0}\sum_{j=1}^{J}\iota_jB_j^2(\boldsymbol{\Omega})+\sum_{j=1}^{J}\frac{1}{4\iota_j}\frac{1}{A_j^2(\boldsymbol{\Omega})}. \quad (34)$$

In fact, the solution to both (33) and (34) is the same. It is noteworthy that if $A_j(\boldsymbol{\Omega})$ is a concave function and $B_j(\boldsymbol{\Omega})$ is a convex one, then the problem (34) is convex quadratic for the given ι_j. Based on the above analysis, the convex problem (34) is solved for a given $\iota_j=\frac{1}{2A_j(\boldsymbol{\Omega})B_j(\boldsymbol{\Omega})}$, and then the value of ι_j will be updated in the next iteration. Consequently, with a specified PS ratio and UAV trajectory, problem P_1 can be represented in the following equivalent manner:

$$\text{P}_6:\min_{\alpha_1[n],\alpha_2[n],\iota[n]>0}\ \sum_{n=1}^{N}\iota[n]P_{\text{sum}}^2[n]+\sum_{n=1}^{N}\frac{1}{4\iota[n]}\frac{1}{R_{\text{sum}}^2[n]} \quad (35)$$

$$s.t.:\frac{\alpha_2[n]|h_{sr}[n]|^2}{\gamma_{\min}[n]}-\alpha_1[n]|h_{sr}[n]|^2\geq\frac{N}{(1-\rho[n])},\forall n, \quad (35a)$$

$$\alpha_2[n]|h_{sd}[n]|^2-\alpha_1[n]|h_{sd}[n]|^2\chi\geq\delta_1^2[n]\chi,\ \forall n, \quad (35b)$$

$$(5a),(5b),(18e),$$

where $\chi=\gamma_{\min}-\eta\rho[n]|h_{sr}[n]|^2|h_{rd}[n]|^2/\delta_2^2[n]$, and $\iota[n]=\frac{1}{2P_{\text{sum}}^2[n]R_{\text{sum}}^2[n]}$. It can be observed that all constraints are linear and convex. Nevertheless, the objective function is non-concave due to the non-concavity of the sum rate function. To deal with this issue, we utilize the result of the following corollary [12].

Corollary 1: Consider $\mathcal{F}$ as a decreasing function, then

$$\min_{\boldsymbol{\Upsilon}\in C}\sum_{j=1}^{J}\mathcal{F}_j\left(\frac{\mathcal{A}_j(\boldsymbol{\Upsilon})}{\mathcal{B}_j(\boldsymbol{\Upsilon})}\right), \quad (36)$$

is equivalent to the following problem:

$$\min_{\boldsymbol{\Upsilon}\in C,\varrho_j}\sum_{j=1}^{J}\mathcal{F}_j(2\varrho_j\sqrt{\mathcal{A}_j(\boldsymbol{\Upsilon})}-\varrho_j^2\mathcal{B}_j(\boldsymbol{\Upsilon})), \quad (37)$$

with the updated value of $\varrho_j=\sqrt{\mathcal{A}_j(\boldsymbol{\Upsilon})}/\mathcal{B}_j(\boldsymbol{\Upsilon})$.

By adopting the result of Corollary 1, the second term of the objective function in P_6 can be equivalently written as:

$$\min_{\alpha_1[n],\alpha_2[n],\varrho[n]}\ \sum_{n=1}^{N}\frac{1}{4\iota[n]}\frac{1}{\hat{R}_{\text{sum}}^2[n]}, \quad (38)$$

where

$$\hat{R}_{\text{sum}}[n]=\log_2(1+\gamma_r^1[n])+\log_2\Big(1+\gamma_d^2[n] \quad (39)$$

$$+2\varrho[n]\sqrt{\alpha_2[n]\ |h_{sd}[n]|^2}-\varrho^2[n](\alpha_1[n]\ |h_{sd}[n]|^2+\delta_1^2[n])\Big),$$

where $\varrho[n]=\frac{\sqrt{\alpha_2[n]\ |h_{sd}[n]|^2}}{\alpha_1[n]\ |h_{sd}[n]|^2+\delta_1^2[n]}$. $\hat{R}_{\text{sum}}[n]$ is now biconcave with respect to the power allocation coefficients and $\varrho[n]$. Accordingly, the multi-convex optimization problem becomes:

$$\text{P}_7:\min_{\boldsymbol{\alpha}[n],\iota[n]}\ \sum_{n=1}^{N}\iota[n]P_{\text{sum}}^2[n]+\sum_{n=1}^{N}\frac{1}{4\iota[n]}\frac{1}{\hat{R}_{\text{sum}}^2[n]} \quad (40)$$

$$s.t.:\quad (5a),(5b),(18e),(35a),(35b),$$

where $\boldsymbol{\alpha}[n]=[\alpha_1[n],\alpha_2[n]]\in\mathbb{R}^{2\times1}$. Note that $P_{\text{sum}}[n]$ is a function of power allocation coefficients, and every coefficient has its own constraint. Hence, the terms of $P_{\text{sum}}[n]$ and $\hat{R}_{\text{sum}}[n]$ are decoupled to optimize $P_{\text{sum}}[n]$ distributively. As a result, the augmented Lagrangian method (ALM), (41), is adopted where a penalty term is added to the Lagrange function of P_7, obtaining a sub-optimal solution. In (41), $\varkappa$ is a penalty factor, and $\{\lambda,\theta,\boldsymbol{\Theta},\phi\}$ are the Lagrange multiplier. Finally, the complexity of the proposed solution comes down to the complexity of solving P_2, P_5 and P_7, whose complexities are $\mathcal{O}(9N^3)$, $\mathcal{O}((8N+3)(5N)^3)$, and $\mathcal{O}(N^2)$, respectively. Therefore, the complexity of the proposed two-stage solution is polynomial of approximately degree four [12].

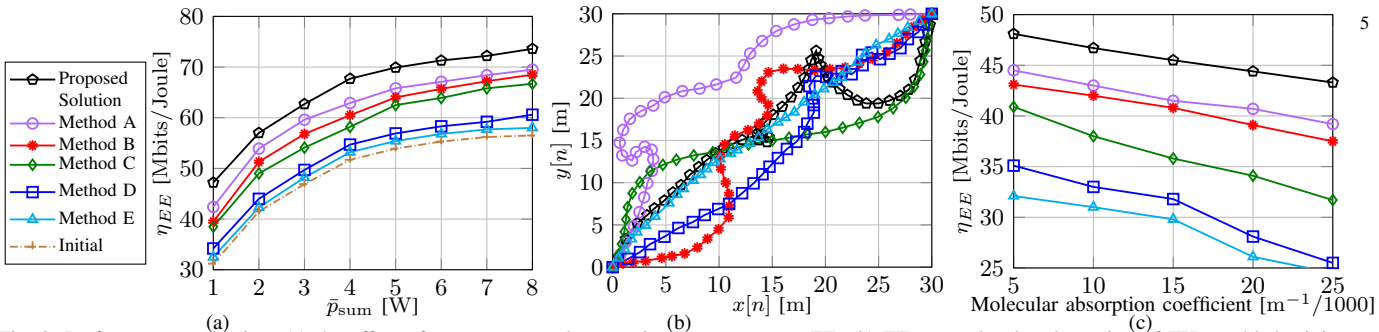

Fig. 2: Performance evaluation: (a) the effect of average network transmit power, $\bar{p}_{\text{sum}}$, on EE, (b) EE vs. molecular absorption of THz-enabled miniature UAV network, (c) the trajectory of miniature UAV in a cooperative THz NOMA-SWIPT network cooperative network.

IV. Simulation Results and Analysis

For simulating the proposed system, a square indoor $30\text{m} \times 30\text{m}$ region is considered, accommodating the user and miniature UAV, both positioned randomly. To avoid peaks in path loss, the carrier frequency is set to $f = 1.2$ THz and the transmission bandwidth to 10 GHz. Considering water vapor's significant influence on molecular absorption loss,we relate the frequency-dependent absorption coefficient $\xi = 0.005$ solely to water vapor molecules [9]. Additionally, $V_{\max} = 1$ m/s, $\varpi = 0.1$ s, $T = 45$ s, $\sigma_2^2 = \delta_1^2[n] = \delta_2^2[n] = -174$ dBm/Hz, $H_1 = 2, H_2 = 3$ m, $P_{\text{peak}} = P_{\max} = 1, P_c = 0.52$ W.

Fig. 2a presents the EE performance as a function of the average network transmission power parameter, $\bar{p}_{\text{sum}} = P_c - P_{\text{EH}} + P_{\max} + P_{\text{peak}}$. The curve marked as 'Initial' represents the EE performance with a non-optimal feasible (random) initialization of the UAV trajectory. Importantly, the proposed solution consistently demonstrates higher performance gaps than other benchmark designs, with the relative gap slightly widening as $\bar{p}_{\text{sum}}$ increases. For comparison, Fig. 2a also investigates the average EE of four methods. Method A investigates the proposed solution based on the NOMA scheme, where the NOMA power coefficient is considered fixed. Method B analyzes the performance superiority between the system's two access schemes, NOMA and OMA. Method C examines the proposed solution with a pre-defined UAV trajectory, while Method D considers the scenario with constant ($\rho[n] = 0.5, \forall n$) PS factors. Method E employs the fractional programming approach from [14], excluding PS factor optimization. Our proposed solution outperforms these benchmarks by $30.3\%, 23.0\%, 21.2\%, 18.1\%, 7.26\%$, and 3.57%, respectively, compared to the case with no trajectory optimization.

Fig. 2b shows the optimized trajectory, while Fig. 2c illustrates the impact of the molecular absorption coefficient on the EE of THz communication schemes under various environmental conditions. Fig. 2c reveals a distinct inverse relationship: as the molecular absorption coefficient increases, indicating higher propagation losses, the EE across all schemes decreases. This phenomenon is attributed to the enhanced signal attenuation due to environmental factors like humidity and temperature, which elevate the molecular absorption. While this increase in absorption can reduce information leakage from miniature UAVs, it concurrently degrades the reception quality at the destination, negatively impacting the overall EE. Notably, despite these challenging conditions, the proposed solution consistently outperforms the baseline methods. This highlights the robustness of the approach, effectively mitigating the adverse effects of increased molecular absorption in maintaining higher EE in THz-enabled UAV networks.

V. Conclusion

In this paper, we have addressed the problem of cooperative cooperative THz-NOMA-enabled miniature UAV network with SWIPT. We have formulated an EE problem to optimize the resource allocation design of the network. To tackle this EE problem, we have proposed an iterative solution design that partitions the original problem into three tractable subproblems based on a two-stage approach. Numerical results highlighted the superiority of the proposed resource allocation algorithm. The comparison with baseline scenarios lacking trajectory, NOMA power, or PS optimization shows the proposed approach improves the system's performance efficiency.

References

[1] H. Müller, V. Niculescu, T. Polonelli, M. Magno, and L. Benini, "Robust and efficient depth-based obstacle avoidance for autonomous miniaturized UAVs," *IEEE Trans. Robot.*, pp. 1–17, 2023.

[2] J. Jalali, A. Khalili, A. Rezaei, J. Famaey, and W. Saad, "Power-efficient antenna switching and beamforming design for multi-user SWIPT with non-linear energy harvesting," in *Proc. IEEE 20th Consumer Commun. Netw. Conf*, pp. 746–751, Las Vegas, NV, USA, 2023.

[3] S. Yin, Y. Zhao, L. Li, and F. R. Yu, "UAV-assisted cooperative communications with power-splitting information and power transfer," *IEEE Trans. Green Commun. Netw*, vol. 3, pp. 1044–1057, Dec. 2019.

[4] X. Sun, W. Yang, and Y. Cai, "Secure communication in NOMA-assisted millimeter-wave SWIPT UAV networks," *IEEE Internet Things J.*, vol. 7, pp. 1884–1897, Mar. 2020.

[5] C. Chaccour, M. N. Soorki, W. Saad, M. Bennis, P. Popovski, and M. Debbah, "Seven defining features of terahertz (THz) wireless systems: A fellowship of communication and sensing," *IEEE Commun. Surv. Tutor.*, vol. 24, pp. 967–993, Q2 2022.

[6] S. B. Melhem and H. Tabassum, "User pairing and outage analysis in multi-carrier NOMA-THz networks," *IEEE Trans. Technol.*, vol. 71, pp. 5546–5551, May 2022.

[7] Q. Li, P. Si, Y. Zhang, J. Wang, D. Zhang, and F. R. Yu, "UAV altitude, relay selection and user association optimization for cooperative relay-transmission in UAV-IRS based THz networks," *IEEE Trans. Green Commun. Netw.*, pp. 1–1, 2023.

[8] N. Iradukunda, Q.-V. Pham, Z. Ding, and W.-J. Hwang, "THz-enabled UAV communications using non-orthogonal multiple access," *IEEE Trans. Veh. Technol.*, vol. 72, pp. 10977–10981, Aug. 2023.

[9] Q. Li, A. Nayak, Y. Zhang, and F. R. Yu, "A cooperative recharging-transmission strategy in powered UAV-aided terahertz downlink networks," *IEEE Trans. Veh. Technol.*, vol. 72, pp. 5479–5484, Apr. 2023.

[10] Y. M. Park, S. S. Hassan, Y. K. Tun, Z. Han, and C. S. Hong, "Joint trajectory and resource optimization of MEC-assisted UAVs in sub-THz networks: A resources-based multi-agent proximal policy optimization drl with attention mechanism,"*IEEETrans.Veh. Technol.*, pp. 1–14, 2023.

[11] C. Chaccour, M. N. Soorki, W. Saad, M. Bennis, and P. Popovski, "can terahertz provide high-rate reliable low-latency communications for wireless VR?,"*IEEE Internet Things J.*, vol. 9, pp. 9712–9729, June 2022.

[12] J. Jalali, A. Khalili, A. Rezaei, R. Berkvens, M. Weyn, and J. Famaey, "IRS-based energy efficiency and admission control maximization for IoT users with short packet lengths," *IEEE Trans. Veh. Technol.*, vol. 72, pp. 12379–12384, Sept. 2023.

[13] Y. Jong, *An efficient global optimization algorithm for nonlinear sum-of-ratios problem*. Center of Natural Science, University of Sciences, Pyongyang, DPR Korea, May 2012.

[14] R. Zhang, R. Tang, Y. Xu, and X. Shen, "Resource allocation for UAV-assisted NOMA systems with dual connectivity," *IEEE Wirel. Commun. Lett.*, vol. 12, pp. 341–345, Feb. 2023.